C. R. Acad. Sci. Paris, Ser. I 353 (2015) 219–224

Contents lists available at ScienceDirect

C. R. Acad. Sci. Paris, Ser. I

www.sciencedirect.com

Ordinary differential equations/Numerical analysis

Numerical analysis of an isotropic phase-field model with magnetic-field effect

Analyse numérique d'un modéle isotrope de champ de phase sous l'effet d'un champ magnétique

Amer Rasheed [a], Abdul Wahab [b]

[a] *Department of Mathematics, School of Science and Engineering, Lahore University of Management Sciences, Opposite Sector U, DHA, Lahore Cantt 54792, Pakistan*
[b] *Department of Mathematics, COMSATS Institute of Information Technology, G.T. Road, 47040, Wah Cantt., Pakistan*

ARTICLE INFO

Article history:
Received 18 November 2014
Accepted 11 December 2014
Available online 6 January 2015

Presented by Philippe G. Ciarlet

ABSTRACT

The aim of this letter is to perform the numerical analysis of an isotropic phase-field model for dendritic solidification of a binary alloy subject to an applied magnetic field in an isothermal environment. Precisely, the numerical stability and error analysis of a finite-element-based approximation scheme are performed. The particular example of a nickel–copper (Ni–Cu) binary alloy is considered. The study substantiates a good agreement between the numerical and theoretical results.

RÉSUMÉ

Le but de cette note est d'effectuer l'analyse numérique d'un modèle isotrope de champ de phase pour la solidification dendritique d'un alliage binaire sous l'effet d'un champ magnétique appliqué dans un environnement isotherme. Précisément, la stabilité numérique et l'analyse d'erreur du schéma d'approximation éléments finis sont effectuées. L'exemple particulier d'un alliage binaire nickel–cuivre (Ni–Cu) est considéré. L'étude montre un bon accord entre les résultats numériques et théoriques.

1. Introduction

The understanding and control over the evolution of dendrites during the solidification process of metals and alloys has a critical impact on the final solidified material [8]. The phase-field models allowed several investigators to unveil the peculiarities of the synthesis and dynamics of materials during the past couple of decades [1,3,8,15,16], albeit these models are unable to render control over dendrite growth and micro-segregation stand-alone. Nevertheless, experimental studies indicate that the control can be procured in the solidification process by virtue of applied external electric and magnetic fields [4,5,7,13].

E-mail addresses: amerasheed@ciitwah.edu.pk, amerasheed@yahoo.com (A. Rasheed), wahab@ciitwah.edu.pk (A. Wahab).

http://dx.doi.org/10.1016/j.crma.2014.12.002
1631-073X/

Recently, Rasheed and Belmiloudi [10–12] developed a phase-field model taking care of convection as well as magnetic field. Primarily, the two-dimensional model by Warren and Boettinger [16] for the nickel–copper (Ni–Cu) binary alloy is considered and then the effects of convection in the phase-field and solute equations, and melt–flow equations in the presence of an externally applied magnetic field are included. We refer to [11] for detailed description of the model and [10] for associated mathematical analysis.

The aim of this note is to provide a numerical scheme based on a finite-element method, and a numerical error and stability analysis for the model proposed by Rasheed and Belmiloudi in an isotropic and isothermal regime. In the next section, we briefly provide the mathematical model. Section 3 is dedicated to the variational formulation. Finally, the stability and error analyses are performed in Section 4.

2. Mathematical formulation

Let $\Omega \subset \mathbb{R}^2$ be a sufficiently smooth open solidification domain with regular boundary $\partial\Omega$ and $t \in (0,T)$ denote the temporal variable with final solidification time T. In the sequel, we entertain the following phase-field model for dendrite solidification due to Rasheed and Belmiloudi [10–12]. Let $\mathbf{u}$, p, ψ, c and $\mathbf{B}$ represent the velocity, pressure, phase, concentration and applied magnetic fields, respectively. Then, in the absence of phase and concentration exchange across, and negligible melt velocity along $\partial\Omega$

$$\begin{cases} \rho_0\big(\partial_t\mathbf{u} + (\mathbf{u}\cdot\nabla)\mathbf{u}\big) = -\nabla p + \mu\Delta\mathbf{u} + \boldsymbol{\mathcal{A}}(\psi,c) + b(\psi)\big((\mathbf{u}\times\mathbf{B})\times\mathbf{B}\big), & \Omega\times(0,T),\\ \nabla\cdot\mathbf{u} = 0, & \Omega\times(0,T),\\ \partial_t\psi + (\mathbf{u}\cdot\nabla)\psi = \epsilon_1\big(\Delta\psi - \mathcal{H}_1^{\lambda,\delta}(\psi,c)\big), & \Omega\times(0,T),\\ \partial_t c + (\mathbf{u}\cdot\nabla)c = \nabla\cdot\big(D(\psi)\nabla c\big) + \nabla\cdot\big(\mathcal{H}_2^{\lambda,\delta}(\psi,c)\nabla\psi\big), & \Omega\times(0,T),\\ (\mathbf{u},\psi,c) = (\mathbf{u}_0,\psi_0,c_0), & \Omega\times\{0\},\\ \mathbf{u}=0, \qquad \nabla\psi\cdot\mathbf{n} = 0, \qquad \nabla c\cdot\mathbf{n} = 0, & \partial\Omega\times(0,T), \end{cases} \tag{1}$$

where ρ_0 and μ are the average density and viscosity, $D(\psi)$ is the diffusion coefficient, $\mathbf{n}$ is the unit outward normal and $\epsilon_1 = M_\psi\epsilon_0^2$ with interface mobility and energy constants $M_\psi > 0$ and ϵ_0. Here $\mathcal{H}_1^{\lambda,\delta}$, $\mathcal{H}_2^{\lambda,\delta}$ and $\boldsymbol{\mathcal{A}}$ are defined by

$$\mathcal{H}_1^{\lambda,\delta}(\psi,c) = \frac{\lambda_1(c)}{\delta^2}g'(\psi) + \frac{\lambda_2(c)}{\delta}\bar{p}'(\psi), \qquad \mathcal{H}_2^{\lambda,\delta} = \alpha_0 D(\psi)c(1-c)\left(\frac{\lambda_1'(c)}{\delta}g'(\psi) - \lambda_2'(c)\bar{p}'(\psi)\right), \tag{2}$$

$$\boldsymbol{\mathcal{A}} = \beta_c a_1(\psi)c\mathbf{G}, \tag{3}$$

and $b(\psi) = \sigma_e a_2(\psi)$ where *prime* denotes the ordinary derivative with respect to the variable involved, σ_e is the electric conductivity, $\mathbf{G}$ is the gravity vector, β_c is the solutal expansion coefficient, δ is the interface thickness, α_0 is a material parameter, λ_i $(i=1,2)$ are linear functions involving material-dependent constants and, g, $\bar{p}$, a_1 and a_2 are included for modeling convenience satisfying the conditions $g(0) = g(1) = 0$, $g'(\psi) = 0 \iff \psi \in \{0,1,1/2\}$, $g''(0), g''(1) > 0$, $g(\psi) = g(1-\psi)$, $\bar{p}(0) = \bar{p}(1) = 0$, $\bar{p}'(\psi) > 0$ for all $\psi \in (0,1)$ and $a_i(0) = 0$ $(i=1,2)$. Throughout this study, we assume $a_i(\psi) = \psi$, $\bar{p}(\psi) = \psi^3(10 - 15\psi + 6\psi^2)$ and $g(\psi) = \bar{p}'(\psi)/30$. We refer the reader to [11] for a detailed exposition.

3. Discrete weak formulation

Let $(\mathbf{u},\mathbf{v}) = \int_\Omega \mathbf{u}\cdot\mathbf{v}\,\mathrm{d}\mathbf{x}$ and define $\mathcal{W} = \{\mathbf{v}\in(H^1(\Omega))^2 \,|\, \mathbf{v}_{\partial\Omega} = 0\}$, $\mathcal{H} = \{q \in L^2(\Omega) \,|\, \int_\Omega q\,\mathrm{d}\mathbf{x} = 0\}$ and $\mathcal{M} = H^1(\Omega)$. Let h be the spatial discretization parameter such that $0 < h < h_0 < 1$ and $\mathcal{T}_h$ be a triangulation of Ω. Consider the $\mathbb{P}_l$, $\mathbb{P}_{l-1}$ and $\mathbb{P}_l$ finite element subspaces $\mathcal{W}_h$, $\mathcal{H}_h$ and $\mathcal{M}_h$ of $\mathcal{W}$, $\mathcal{H}$ and $\mathcal{M}$ respectively over $\mathcal{T}_h$, where $\mathbb{P}_l$ is the space of polynomials with total degree at most l. Furthermore, we make the following assumptions.

(A1) $\exists c_1 > 0$ s.t. $\forall\mathbf{X} = (\mathbf{u},\psi,c) \in (H^{r+1}(\Omega))^4 \cap (\mathcal{W}\times\mathcal{M}^2)$ and $r \in [1,l]$,

$$\inf_{\mathbf{X}_h\in\mathcal{W}_h\times\mathcal{M}_h^2} \|\mathbf{X}-\mathbf{X}_h\| \le c_1 h^r \|\mathbf{X}\|_{H^{r+1}(\Omega)}.$$

(A2) $\exists c_2 > 0$ s.t. $\forall q \in H^r(\Omega)\cap\mathcal{H}$ and $r\in[1,l]$, $\inf_{q_h\in\mathcal{H}_h}\|q-q_h\| \le c_2 h^r\|q\|_{H^r(\Omega)}$.

(A3) $\exists c_3 > 0$ s.t. (*Inf–Sup condition*) $\inf_{q_h\in\mathcal{H}_h}\sup_{\mathbf{v}_h\in\mathcal{W}_h}\frac{c_p(\mathbf{v}_h,q_h)}{\|\mathbf{v}_h\|\|q_h\|} \ge c_3$, where $c_p(\mathbf{u},p) = -(\nabla\cdot\mathbf{u},p)$.

(A4) Let $\mathbf{X}_0 = (\mathbf{u}_0,\psi_0,c_0) \in (H^{r+1}(\Omega))^4$ for $r\in[1,l]$, then $h\|\mathbf{X}_0 - \mathbf{X}_{0h}\| + |\mathbf{X}_0 - \mathbf{X}_{0h}| \le c_4 h^{r+1}$, where $\mathbf{X}_{0h} = (\mathbf{u}_{0h},\psi_{0h},c_{0h}) \in \mathcal{W}_h\times\mathcal{M}_h^2$ is the approximation of $\mathbf{X}_0$.

(A5) For all integers $\mathfrak{m},\mathfrak{p},\mathfrak{q}$ and $\mathfrak{k}$ with $0 < \mathfrak{p},\mathfrak{q} \le \infty$ and for all simplex $K\in\mathcal{T}_h$, we have:

$$\|\mathbf{X}_h\|_{W^{\mathfrak{m},\mathfrak{q}}(K)} \le c_4 h^{n/\mathfrak{q}-n/\mathfrak{p}+\mathfrak{k}-\mathfrak{m}}\|\mathbf{X}_h\|_{W^{\mathfrak{k},\mathfrak{p}}(K)}, \quad \forall\mathbf{X}_h\in\mathcal{W}_h\times\mathcal{M}_h^2.$$

Consider the following discrete weak form of (1), wherein we use artificial source terms F_u, F_ψ and F_c for fabricating exact solutions thereby analyzing the convergence and stability of the numerical scheme.

Discrete weak form Find $(\mathbf{u}_h, p_h, \psi_h, c_h) \in \mathcal{W}_h \times \mathcal{H}_h \times \mathcal{M}_h \times \mathcal{M}_h$ such that $\forall (\mathbf{v}_h, q_h, \varphi_h, z_h) \in \mathcal{W}_h \times \mathcal{H}_h \times \mathcal{M}_h \times \mathcal{M}_h$

$$\begin{cases} \rho_0(\partial_t \mathbf{u}_h, \mathbf{v}_h) + a_u(\mathbf{u}_h, \mathbf{v}_h) + b_u(\mathbf{u}_h, \mathbf{u}_h, \mathbf{v}_h) + c_p(\mathbf{v}_h, p_h) - \big(\boldsymbol{\mathcal{A}}(\psi_h, c_h), \mathbf{v}_h\big) \\ \quad -\big(b(\psi_h)\big((\mathbf{u}_h \times \mathbf{B}) \times \mathbf{B}\big), \mathbf{v}_h\big) = (\mathbf{F}_u, \mathbf{v}_h), \\ c_p(\mathbf{u}_h, q_h) = 0, \\ (\partial_t \psi_h, \varphi_h) + a_\psi(\psi_h, \varphi_h) + b_\psi(\mathbf{u}_h, \psi_h, \varphi_h) + \epsilon_1\big(\mathcal{H}_1^{\lambda,\delta}(\psi_h, c_h), \varphi_h\big) = (F_\psi, \varphi_h), \\ (\partial_t c_h, z_h) + b_c(\mathbf{u}_h, c_h, z_h) + \big(D(\psi_h)\nabla c_h, \nabla z_h\big) + \big(\mathcal{H}_2^{\lambda,\delta}(\psi_h, c_h)\nabla\psi_h, \nabla z_h\big) = (F_c, z_h), \\ (\mathbf{u}_h, \psi_h, c_h)(t=0) = (\mathbf{u}_{0h}, \psi_{0h}, c_{0h}), \\ a_u(\mathbf{u}, \mathbf{v}) = \mu \displaystyle\int_\Omega \nabla\mathbf{u} \cdot \nabla\mathbf{v}\, \mathrm{d}\mathbf{x}, \qquad a_\psi(\psi, \phi) = \epsilon_1 \int_\Omega \nabla\psi \cdot \nabla\phi\, \mathrm{d}\mathbf{x}, \qquad b_c(\mathbf{u}, c, z) = \sum_{i=1}^2 \int_\Omega u_i(\partial_i c) z\, \mathrm{d}\mathbf{x}, \\ b_u(\mathbf{u}, \mathbf{v}, \mathbf{w}) = \rho_0 \displaystyle\sum_{i,j=1}^2 \int_\Omega u_i(\partial_i v_j) w_j\, \mathrm{d}\mathbf{x}, \qquad b_\psi(\mathbf{u}, \psi, \phi) = \sum_{i=1}^2 \int_\Omega u_i(\partial_i \psi)\phi\, \mathrm{d}\mathbf{x}. \end{cases} \tag{4}$$

Let $(\varphi_{ih})_1^M$, $(q_{ih})_{2M+1}^{2M+N}$ and $(z_{ih})_{2M+N}^{2M+N+\tilde{M}}$ be the basis of $\mathcal{W}_h$, $\mathcal{H}_h$ and $\mathcal{M}_h$ respectively and

$$\mathbf{u}_h = \sum_{i=1}^M \mathbf{u}_{ih}\varphi_{ih} = \sum_{i=1}^M u_{ih}\underline{\varphi}_{ih}^u + \sum_{i=1}^M v_{ih}\underline{\varphi}_{ih}^v, \qquad p_h = \sum_{i=2M+1}^{2M+N} p_{ih} q_{ih}, \tag{5}$$

$$\psi_h = \sum_{i=2M+N+1}^{2M+N+\tilde{M}} \psi_{ih} z_{ih}, \qquad c_h = \sum_{i=2M+N+\tilde{M}+1}^{2M+N+2\tilde{M}} c_{ih} z_{ih}, \tag{6}$$

where $\mathbf{u}_{ih} = (u_{ih} \quad v_{ih})^{\mathrm{t}}$, $\underline{\varphi}_{ih}^u = (\varphi_{ih} \quad 0)^{\mathrm{t}}$, $\underline{\varphi}_{ih}^v = (0 \quad \varphi_{ih})^{\mathrm{t}}$.

By virtue of (5), the semi-discrete weak form (4) yields the differential–algebraic system

$$\mathbb{M}\frac{\mathrm{d}\mathbf{Y}_h}{\mathrm{d}t} + \mathbb{A}(\mathbf{Y}_h)\mathbf{Y}_h + \mathbf{L}(\mathbf{Y}_h) = \mathbf{R}, \qquad \mathbf{Y}_h(t=0) = \mathbf{Y}_{0h}, \tag{7}$$

$$\mathbf{Y}_h = (\mathbf{u}_{1h} \cdots \mathbf{u}_{Mh} \quad p_{1h} \cdots p_{Nh} \quad \psi_{1h} \cdots \psi_{\tilde{M}h} \quad c_{1h} \cdots c_{\tilde{M}h})^{\mathrm{t}}, \tag{8}$$

where $\mathbf{R} = (R_1\ 0\ R_3\ R_4)^{\mathrm{t}}$, $\mathbf{L}(Y_h) = (L_1\ 0\ L_3\ 0)^{\mathrm{t}}$ and, for $K_1 = 2M + N + 2\tilde{M}$ and $K_2 = 2M + N + 2\tilde{M}$

$$\mathbb{M} = \begin{pmatrix} M_{11} & 0 & 0 & 0 \\ 0 & 0 & 0 & 0 \\ 0 & 0 & M_{33} & 0 \\ 0 & 0 & 0 & M_{44} \end{pmatrix} \in \mathbb{R}^{K_1 \times K_2}, \qquad \mathbb{A}(\mathbf{Y}_h) = \begin{pmatrix} A_{11} & A_{12} & 0 & 0 \\ A_{21} & 0 & 0 & 0 \\ 0 & 0 & A_{33} & 0 \\ 0 & 0 & A_{43} & A_{44} \end{pmatrix} \in \mathbb{R}^{K_1 \times K_2},$$

with

$$\begin{aligned} &(M_{11})_{ji} = \rho_0\big(\underline{\varphi}_{ih}^u, \underline{\varphi}_{jh}^u\big) + \rho_0\big(\underline{\varphi}_{ih}^v, \underline{\varphi}_{jh}^v\big), \qquad (M_{33})_{ji} = (z_{ih}, z_{jh}), \qquad (M_{44})_{ji} = (z_{ih}, z_{jh}), \\ &(A_{11})_{ji} = a_u\big(\underline{\varphi}_{ih}^u, \underline{\varphi}_{jh}^u\big) + a_u\big(\underline{\varphi}_{ih}^v, \underline{\varphi}_{jh}^v\big) + b_u\big(\mathbf{u}_h; \underline{\varphi}_{ih}^u, \underline{\varphi}_{jh}^u\big) + b_u\big(\mathbf{u}_h, \underline{\varphi}_{ih}^v, \underline{\varphi}_{jh}^v\big) \\ &\qquad\qquad - \big(b(\psi_h)\big((\underline{\varphi}_{ih}^u \times \mathbf{B}) \times \mathbf{B}\big), \underline{\varphi}_{jh}^u\big) - \big(b(\psi_h)\big((\underline{\varphi}_{ih}^v \times \mathbf{B}) \times \mathbf{B}\big), \underline{\varphi}_{jh}^v\big), \\ &(A_{12})_{ji} = \big(q_{ih}, \nabla \cdot \big(\underline{\varphi}_{jh}^u\big)\big) + \big(q_{ih}, \nabla \cdot \underline{\varphi}_{jh}^v\big) = (A_{21})_{ij}, \qquad (A_{33})_{ji} = a_\psi(z_{ih}, z_{jh}) + b_\psi(\mathbf{u}_h, z_{ih}, z_{jh}), \\ &(A_{43})_{ji} = \big(\mathcal{H}_2^{\lambda,\delta}(\psi_h, c_h)\nabla z_{ih}, \nabla z_{jh}\big), \qquad (A_{44})_{ji} = \big(D(\psi_h)\nabla z_{ih}, \nabla z_{jh}\big) + b_c(\mathbf{u}_h, z_{ih}, z_{jh}), \\ &(L_1)_j = \big(\boldsymbol{\mathcal{A}}_1(\psi_h, c_h), \underline{\varphi}_{jh}^u\big) + \big(\boldsymbol{\mathcal{A}}_1(\psi_h, c_h), \underline{\varphi}_{jh}^v\big), \qquad (L_3)_j = \epsilon_1\big(\mathcal{H}_1^{\lambda,\delta}(\psi_h, c_h), z_{jh}\big), \\ &(R_1)_j = \big(\mathbf{F}_u, \underline{\varphi}_{jh}^u\big) + \big(\mathbf{F}_u, \underline{\varphi}_{jh}^v\big), \qquad (R_3)_j = (F_\psi, z_{jh}), \qquad (R_4)_j = (F_c, z_{jh}). \end{aligned}$$

Let $\mathbf{u}_i = \mathbf{u}(t_i)$, $t_i = i\tau$ $(0 \le i \le k)$ where τ is the temporal step size, $\Psi_h = (\mathbf{u}_h, \psi_h, c_h)$, $\Psi = (\mathbf{u}, \psi, c)$ and $\mathbb{Y}$ be a Banach space. We define

$$\ell^p(0, T, \mathbb{Y}) = \left\{ \mathbf{u} : (t_1, \cdots, t_k) \to \mathbb{Y} \;\middle|\; \|\mathbf{u}\|_{\ell^p(0,T,\mathbb{Y})}^p = \left(\tau \sum_{i=1}^k \|\mathbf{u}_i\|_{\mathbb{Y}}^p\right) < \infty \right\}.$$

Then, the following error estimates can be obtained; see, for instance, [2,9,14]

$$\|\Psi_h - \Psi\|_{\ell^2(0,T,L^2(\Omega))} \le C\big(\tau^\alpha + h^{\beta_1}\big) \quad \text{and} \quad \|p_h - p\|_{\ell^2(0,T,L^2(\Omega))} \le C\big(\tau^\alpha + h^{\beta_2}\big), \tag{9}$$

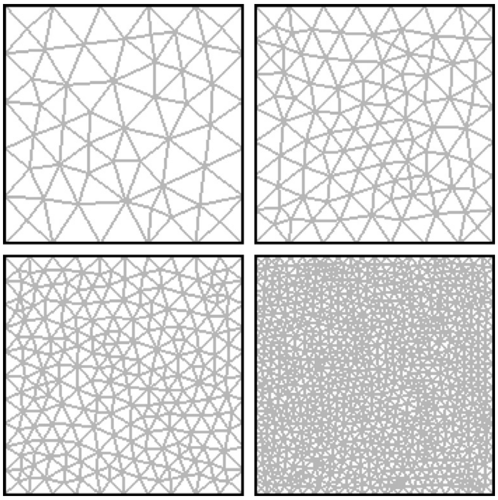

Fig. 1. Meshes.

Table 1
Mesh statistics.

Mesh	h	Elements	Boundary elements
1	0.2	106	5
2	0.15	200	7
3	0.1	434	10
4	0.05	1712	20

for some $\beta_1, \beta_2 > 1$ and $\alpha \geq 1$. Note that β_i $(i = 1, 2)$ are less than the minimum degree of the finite elements (polynomials) and the Sobolev space regularity of the solutions. Moreover, for optimal spatial (resp. temporal) convergence rate $\tau \leq h^{\beta_i}$ (resp. $h^{\beta_i} < \tau$).

4. Analysis of the numerical scheme

In this section, we analyze numerical error and stability to validate the numerical scheme. The system (7) is fully discretized first by invoking Euler's backward difference method and then resolved by using the Newton iteration technique on the resulting non-linear fixed-point system, whereas we have made use of the solver DASSL [6]. The values of the physical parameters are consistent with that in [16] and the constants for the melt–flow equations are chosen in accordance with the physical properties of the nickel–copper (Ni–Cu) system; see, for example [9,11].

In the sequel, we choose $T = 1$, $\Omega = [0, 2\pi] \times [0, 2\pi]$, $\mathbf{B} = \frac{1}{\sqrt{2}}(1, 1)$ and entertain the following fabricated exact solution to (1) obtained by exploiting the artificial source terms $\mathbf{F}_u$, F_ψ and F_c,

$$\mathbf{u}_{\text{ex}} = \left(\tfrac{2e^{1-t}}{4\pi^2} \sin(x)^2 y(1 - \tfrac{y}{2\pi})(1 - \tfrac{y}{\pi}) \quad -\tfrac{2e^{1-t}}{4\pi^2} \sin(x)\cos(x) y^2 (1 - \tfrac{y}{2\pi})^2 \right)^t,$$

$$p_{\text{ex}} = e^{1-t}\cos(y), \qquad \psi_{\text{ex}} = \frac{e^{1-t}}{2}\big(\cos(x)\cos(y) + 1\big), \qquad c_{\text{ex}} = \frac{2e^{1-t}}{\pi^2} x^2 \left(1 - \frac{x}{2\pi}\right)^2 \big(\cos(y) + 1\big).$$

Furthermore, we consider a sequence of four meshes with a decreasing step h (see Fig. 1 and Table 1) and use Lagrange $\mathbb{P}_2$ elements for velocity, phase-field and concentration, and $\mathbb{P}_1$ elements for pressure.

4.1. Numerical error analysis

In Fig. 2, L^2-norms of errors in $\mathbf{u}$, p, ψ and c are plotted versus h (left) and τ (right) in *log*-scales. For h-curves, we used $\tau = 0.01$ and 0.001 for linear and quadratic elements, respectively. It is observed that the slopes of the error curves for velocity, phase-field and concentration are approximately 3, whereas that for the pressure is 2; refer to Table 2. For τ-curves slopes of all the curves are approximately 1, i.e. $\alpha = 1$. Both of theses numerical estimates are in good agreement with the postulated error estimate (9).

4.2. Numerical stability analysis

In order to ascertain the numerical stability of the model, we include $(1 - \epsilon\,\text{randf})$ in the artificial source terms to introduce ϵ-perturbations in the numerical solution, where random function randf assumes values in $[0, 1]$ and ϵ is the perturbation control parameter. We fix $h = 0.2$ and $\tau = 0.1$.

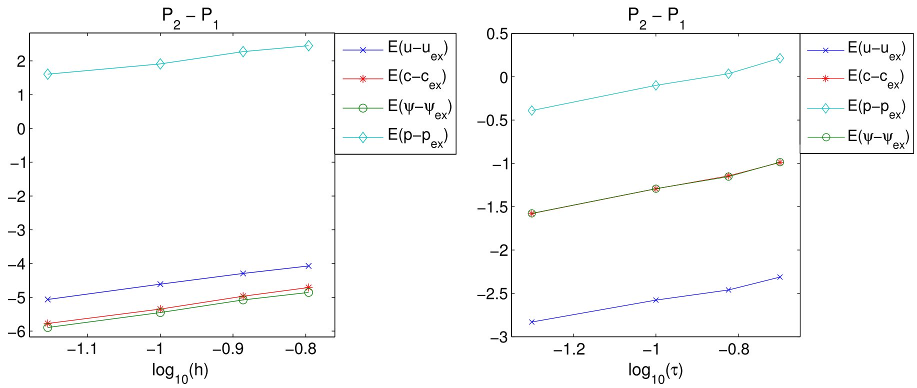

Fig. 2. (Color online.) Error curves with respect to spatial (left) and temporal (right) step size.

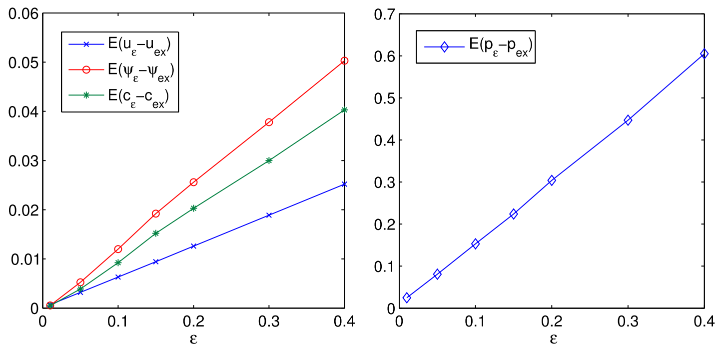

Fig. 3. (Color online.) $E(\Phi_\epsilon - \Phi_{\text{ex}})$ versus ϵ.

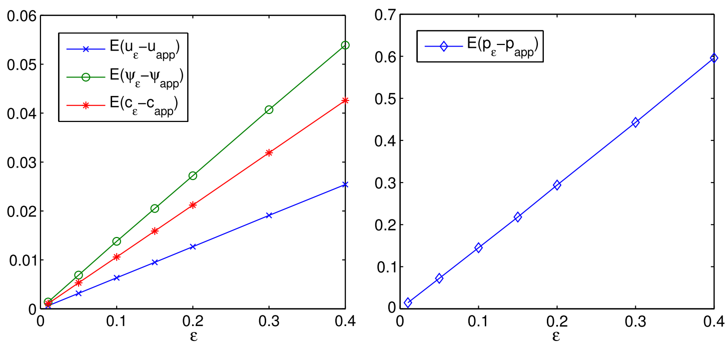

Fig. 4. (Color online.) $E(\Phi_\epsilon - \Phi_{\text{app}})$ versus ϵ.

Table 2
Estimated β_i, $i = 1, 2$.

β_1 for $\mathbf{u}$ with $\mathbb{P}_2$	2.7501
β_2 for p with $\mathbb{P}_1$	1.8426
β_1 for ψ with $\mathbb{P}_2$	2.8001
β_1 for c with $\mathbb{P}_2$	2.8449

Table 3
Slopes of norm L_2.

Slope	$E(\Phi_\epsilon - \Phi_{\text{ex}})$
$m_{\mathbf{u}}$	0.0628
m_ψ	0.1276
m_c	0.1021
m_p	1.4738

We perform three different stability tests in Figs. 3–5. In Fig. 3, the L^2-norm of the discrepancy between exact solution $\Phi_{\text{ex}} = (\mathbf{u}_{\text{ex}}, p_{\text{ex}}, \psi_{\text{ex}}, c_{\text{ex}})$ and its ϵ-perturbation $\Phi_\epsilon = (\mathbf{u}_\epsilon, p_\epsilon, \psi_\epsilon, c_\epsilon)$, i.e. $E(\Phi_\epsilon - \Phi_{\text{ex}}) = \|\Phi_\epsilon - \Phi_{\text{ex}}\|_{L_2}$ is plotted versus ϵ. A linear dependence of error on ϵ is observed, indeed, $E(\Phi_\epsilon - \Phi_{\text{ex}}) \approx m_s \epsilon$ where m_s $(s = u, p, \psi, c)$ represents the slope of the error curve; refer to Table 3. In Fig. 4, $E(\Phi_\epsilon - \Phi_{\text{app}}) = \|\Phi_\epsilon - \Phi_{\text{app}}\|_{L_2}$ is plotted against ϵ where $\Phi_{\text{app}} = (\mathbf{u}_{\text{app}}, p_{\text{app}}, \psi_{\text{app}}, c_{\text{app}})$ is the approximate solution without random error (i.e. $\epsilon = 0$). The same observation holds as in Fig. 4; refer also to Table 4. Finally, in Fig. 5, the solution curves for different perturbation levels ϵ are delineated on a part of the domain in order to establish stability with respect to random perturbations. We fix $t = 1$, $y = \pi$ and $x \in [0, 1]$ for velocity and, $t = 1$, $x = \pi$ and $y \in [0, 1]$ for pressure, phase field and concentration. The graphs substantiate that the solution is indeed stable.

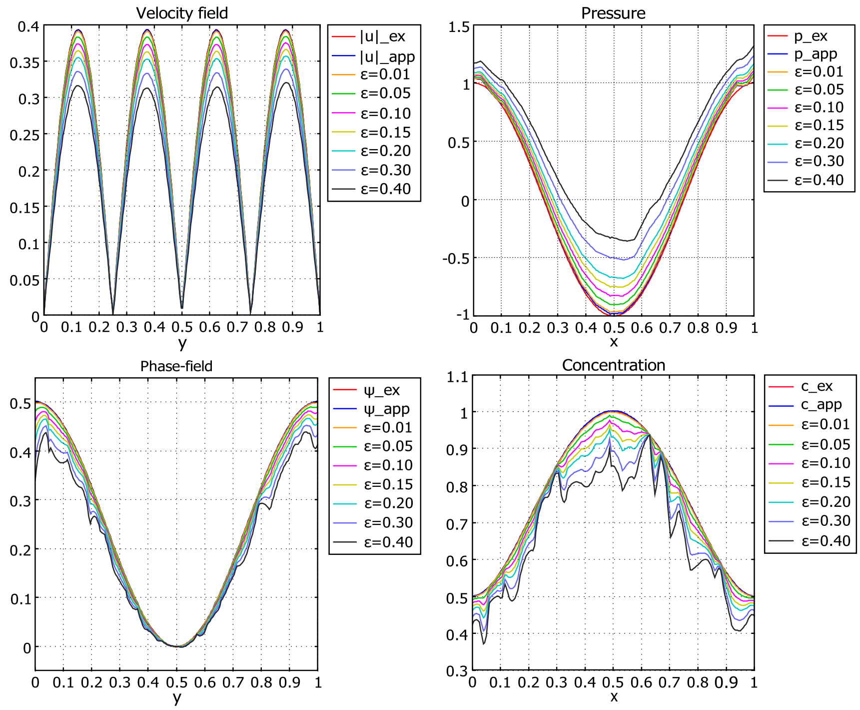

Fig. 5. (Color online.) Solution curves for the different values of ϵ.

Table 4
Slopes of norm L_2.

Slope	$E(\Phi_\epsilon - \Phi_{\text{app}})$
$m_{\mathbf{u}}$	0.0628
m_ψ	0.1277
m_c	0.1028
m_p	1.4913

References

[1] M.D. Anderson, G.B. McFadden, A.A. Wheeler, A phase-field model of solidification with convection, Physica D 135 (2000) 175–194.
[2] A. Belmiloudi, Method of characteristics and error estimates of the perturbation of given mean flow, in: Application of Mathematics in Engineering and Business Sozopol, Proc. XXIInd Summer School, 1996, pp. 25–38.
[3] M. Grujicic, G. Cao, R.S. Millar, Computer modelling of the evolution of dendrite microstructure in binary alloys during non-isothermal solidification, J. Mater. Synth. Process. 10 (2002) 191–203.
[4] H.B. Hadid, D. Henry, S. Kaddeche, Numerical study of convection in the horizontal Bridgman configuration under the action of a constant magnetic field. Part 1. Two-dimensional flow, J. Fluid Mech. 333 (1997) 23–56.
[5] M. Li, T. Takuya, N. Omura, K. Miwa, Effects of magnetic field and electric current on the solidification of AZ91D magnesium alloys using an electromagnetic vibration technique, J. Alloys Compd. 487 (2009) 187–193.
[6] L.R. Petzold, A description of DASSL: a differential/algebraic system solver, in: Scientific Computing, IMACS Trans. Sci. Comput., 1983, pp. 65–68.
[7] P. Prescott, F. Incropera, Magnetically damped convection during solidification of a binary metal alloy, Trans. Amer. Soc. Mech. Eng. 115 (1993) 302–310.
[8] J.C. Ramizer, C. Beckermann, Examination of binary alloy free dendritic growth theories with a phase-field model, Acta Mater. 53 (2005) 1721–1736.
[9] A. Rasheed, Dendritic solidification of binary mixtures of metals under the action of magnetic field: modeling, mathematical and numerical analysis, Ph.D. dissertation, INSA de Rennes, France, 2010.
[10] A. Rasheed, A. Belmiloudi, An analysis of the phase-field model for isothermal binary alloy solidification with convection under the influence of magnetic field, J. Math. Anal. Appl. 390 (2012) 244–273.
[11] A. Rasheed, A. Belmiloudi, Mathematical modelling and numerical simulation of dendrite growth using phase-field method with a magnetic field effect, Commun. Comput. Phys. 14 (2013) 477–508.
[12] A. Rasheed, A. Belmiloudi, F. Mahé, Dynamics of dendrite growth in a binary alloy with magnetic field affect, Discrete Contin. Dyn. Syst. (2011) 1224–1233 (special issue).
[13] R. Sampath, The adjoint method for the design of directional binary alloy solidification processes in the presence of a strong magnetic field, Ph.D. dissertation, Cornell University, Ithaca, NY, USA, 2001.
[14] E. Süli, Convergence and non-linear stability of Lagrange–Galerkin method for the Navier–Stokes equations, Numer. Math. 53 (1988) 459–483.
[15] X. Tong, C. Beckermann, A. Kerma, Q. Li, Phase-field simulations of dendritic crystal growth in a forced flow, Phys. Rev. E 63 (2001) 061601.
[16] J.A. Warren, W.J. Boettinger, Prediction of dendritic growth and microsegregation patterns in a binary alloy using the phase-field method, Acta Metall. Mater. 43 (1995) 689–703.